Investigation of decay mechanisms and associated aspects of exotic nobelium isotopes using the Skyrme energy density formalism[*]

Shubhpreet Kaur[†] [ID]   Raj Kumar   Manoj K. Sharma

Department of Physics and Materials Science, Thapar Institute of Engineering and Technology, Patiala 147004, India

Abstract: The search for heavy elements has yielded many surprises and enhanced our knowledge of nuclear synthesis and associated dynamical aspects. Although new elements and their associated isotopes have been synthesized, information concerning elements with $Z \geq 102$, remains scarce. Further, concerning the transfermium elements, the nuclear shell structure is key to ensuring nuclear stability. Hence, the shell effects have key implications on such nuclei. Many experimental and theoretical investigations have been conducted to examine the reactions induced by heavy ions and the subsequent decay mechanisms in the superheavy mass region. In addition, the region of transfermium elements is of great interest because of the neutron/proton shell effects. Here, our objective is to analyze the decay mechanisms of nuclides having $Z = 102$ nuclei, *i.e.,* ^{248}No* and ^{250}No*. An extensive study was conducted using the dynamical cluster-decay model (DCM) based on Quantum Mechanical Fragmentation Theory (QMFT). The focus was to investigate compound nucleus (CN) and non-compound nucleus (nCN) mechanisms, including fusion-fission (ff), quasi-fission (QF), and fast fission (FF). The specific isotopes of interest are ^{248}No* and ^{250}No*, with attention given to the role of the center-of-mass energy ($E_{\text{c.m.}}$) and angular momentum (ℓ). The nuclear interaction potential was derived using the Skyrme energy density formalism (SEDF) with the GSkI force parameters. The capture cross-sections were calculated using the ℓ-summed Wong Model. The determination of the probability of compound nucleus formation (P_{CN}) involved a function that is dependent upon the center-of-mass energy. The lifetimes of the ff and QF channels were also investigated. Here, CN and nCN decay mechanisms for two isotopes of $Z = 102$ nobelium were analyzed over the range of center-of-mass values ($E_{\text{c.m.}}$) considering the quadrupole deformation (β_2) and optimum orientations ($\theta_{\text{opt.}}$) of the decaying fragments. The fragmentation potential, preformation probability, neck length parameter, and reaction cross-sections were explored. Further, P_{CN} was calculated to determine the mechanisms of decay of ^{248}No* and ^{250}No* isotopes. The obtained fusion–fission lifetimes and quasi-fission lifetimes are compared with the dinuclear system (DNS) approach. Among the considered isotopes having $Z = 102$, *i.e.*, the ^{248}No* formed in the ^{40}Ca + ^{208}Pb reaction and ^{250}No* formed via two different entrance channels, ^{44}Ca+^{206}Pb and ^{64}Ni+^{186}W, show asymmetric fragmentation with the effect of β_2 deformation at the energies beyond the Coulomb barrier. Of note, the nCN (QF and FF) decay mechanisms compete with the CN fission channels. The calculations based on the DCM show a strong correlation with the experimental data. The most probable fragments, such as ^{122}Sn and ^{128}Te, were observed near the magic shell closure at $Z = 50$ and $N = 82$. Further, as the excitation energy increased, the fusion–fission and quasi-fission lifetimes decreased.

Keywords: super heavy nuclei, $Z = 102$, cross-sections, lifetimes

I. INTRODUCTION

The study of superheavy elements and their synthesis has become an important field of research recently. To date, elements up to $Z = 118$ and their corresponding isotopes have been synthesized. However, research into the superheavy nuclei beyond fermium has received much attention in the last few decades because these nuclei are classified as transfermium elements, whose stability is mostly governed by shell effects. The quest to find the heaviest element in the nuclear landscape has yielded many surprises and expanded our understanding of nuclear reactions. These reactions play a pivotal role in the extension of the Periodic Table via the synthesis of new elements and isotopes. Numerous theoretical and experimental endeavors have been conducted to explore vari-

ous reaction conditions and the mechanisms that govern their subsequent decay [1−10].

The study of the disintegration of a compound nucleus formed through various low-energy heavy-ion reactions is a fascinating topic because it facilitates the production of new, non-natural isotopes. Furthermore, these mechanisms provide us with a thorough understanding of many aspects of nuclear reactions and their associated structural effects. Decay dynamics is widely used to explore the compound (CN) and non-compound nucleus (nCN) decay mechanisms. The equilibrated state of the composite system in a heavy-ion reaction (HIR) is influenced by several factors, including the mass asymmetry of the entrance channel (α), Businaro–Gallone mass asymmetry (α_{BG}) [11, 12], incident energy required to overcome the Coulomb barrier, product of charges of the projectile and target ($Z_P Z_T$), deformations and orientations, and shell effects.

Because the colliding massive nuclei experience an enhancement in the Coulomb repulsion, it may result in decay of the composite system. When a composite system reaches full equilibrium, the projectile and target merge, resulting in the formation of a CN stage. Next, two decay routes are possible: evaporation residue (ER) or fusion–fission (ff) fragments. In contrast, a non-equilibrated fused system, *i.e.,* nCN undergoes separation by transferring only a small number of nucleons. Consequently, different decay mechanisms emerge, such as quasi fission (QF), fast fission (FF), and pre-equilibrium fission (PEF), *etc.* [13].

The fusion cross-sections in superheavy elements are significantly suppressed by a non-equilibrium process, *i.e.,* QF. The process involves the formation of a dinuclear system, which then divides into two fragments resembling fission, with the original kinetic energy being mostly or entirely dissipated. The QF process occurs rapidly, typically within 10^{-21} s, before the formation of a compact CN. Quasi-fission can be classified into two categories based on the shell effects of the fission fragments. Asymmetric QF occurs when there are proton shell closures at $Z = 28$ and 82, as well as neutron shell closures at $N = 50$ and 126. On the other hand, symmetric QF occurs when there are shell closures at $Z = 50$ and $N = 82$. Fast fission is a nuclear chain-reaction mechanism that occurs when the potential barrier is eliminated because of a significant centrifugal force, especially at high angular momentum. Therefore, these processes have been examined to elucidate the decay dynamics of HIR in the heavy and superheavy mass regions.

Lifetime estimation provides a comprehensive indication of the nuclear reaction mechanism. The attributes of the fissioning nucleus, such as its fissility and excitation energy, are crucial for determining the lifetime of the decay process. Processes such as QF often happen within a short timescale of around 10^{-21} to 10^{-20} s, whereas FF takes place over longer durations, roughly 10^{-20} to 10^{-16} s. The syntheses of the heavy and superheavy elements are strongly hindered by the nCN processes that result in fast splitting of the CN; hence, many studies have focused on the timescales of such processes. This work aims to assess the timescales of QF and ff using the dynamical cluster-decay model (DCM) and compare the results obtained using a dinuclear system (DNS) model. Further, the lifetimes obtained in the DNS approach are greatly affected by the charge of the projectile and target nuclei and beam energy, *etc.* and the DNS lifetime must be sufficient to achieve the complete fusion of the interacting nuclei. Hence, lifetime calculations were carried out, and the results are compared for both approaches. The overall aim of the study is to investigate the decay mechanisms of CN and nCN. A few examples of such can be found in references [14−28]. Further, to study the nuclear interaction potential, the Skyrme energy density formalism (SEDF) was used with the frozen density approximations, adopting the GSkI parameters. The Skyrme Hamiltonian density comprises distinct components that highlight the finite characteristics of nuclei. Recent advancements in the Skyrme Hamiltonian density have incorporated supplementary terms that are particularly useful for investigating nuclei that are highly responsive to the isospin-rich areas and nuclei with neutron–proton asymmetry [29]. The SEDF has been successfully applied in the light and heavy mass regions, and it would be interesting to investigate the effect of the SEDF nuclear potential in the superheavy mass regions and explore its properties. The nobelium isotope nuclei fall in the superheavy mass region. Hence, it would be intriguing to study its properties using the SEDF.

Recent studies related to nobelium nuclei are as follows: ff analysis of $^{12}C+^{248}Cm$ and $^{16}O+^{244}Pu$ nuclear reactions across the Coulomb barrier by Vijay *et al.* [30] and the assessment of the evaporation residue cross-section in the decay of $^{254}No^*$ formed in $^{206}Pb+^{48}Ca$ by Niyti *et al.* [31]. Recently, Yu-Hai Zhang *et al.* studied the production cross-sections of $^{243-248}No$ isotopes in fusion reactions [32]. In addition, the different decay modes and half-life of nobelium isotopes have been investigated by Bayram *et al.* [33]. Further related works can be found in references [34, 35].

There has been a significant increase in interest in the CN and nCN mechanisms recently. This is primarily because these reactions could be used to synthesize a wide range of heavy and superheavy elements. However, identifying the impact of CN and nCN processes in different decay channels has consistently been a challenge. This is primarily because experimental evidence related to these channels either overlap or their contributions are not clear. Here, the DCM using the SEDF with GSkI parameter sets was used to analyze the respective contributions of different fission decay mechanisms in the processes of CN and nCN in $^{248}No^*$ and $^{250}No^*$ isotopes of $Z = 102$ nuclei over a range of center-of-mass energies around the Coulomb barrier based on the experimental

finding of Kozulin *et al.* [36] and Knyazheva *et al.* [37]. Further, the fission peaks and the reaction cross-sections were studied by including deformation effect up to quadrupole (β_2) deformations. As a result, the effect of octupole deformation in the fission peaks within the low-energy range at different excitation energies can be observed [38, 39].

The organization of this paper is as follows: In Sec. II, we explain the theoretical framework employed in this study. Specifically, the SEDF [29, 40, 41] in reference to the DCM and the ℓ-summed Wong model [42]. Additionally, the probability of compound nucleus formation (P_{CN}) using an energy-dependent function is considered [36, 43], and we examine the lifetimes using a theoretical approach derived from DNS calculations [44, 45]. Section III comprises the findings and analysis, and Sec. IV provides a summary of the work.

II. METHODOLOGY

A. Dynamical Cluster-decay Model (DCM)

Used to investigate the various nuclear mechanisms, the Quantum Mechanical Fragmentation Theory (QMFT)-based [46−48] DCM [14, 15, 20−28] is framed around the terms of collective coordinates of mass and charge asymmetry, relative separation coordinate, 'R', deformations $\beta_{\lambda i}(\lambda = 2, 3, 4$ and $i = 1, 2)$, orientations of the deformed fragments, θ_i ($i = 1,2$), and the neck parameter (ΔR). The mass and charge asymmetry are given, respectively, as follows.

$$\eta_A = \frac{A_1 - A_2}{A_{CN}}, \quad \eta_Z = \frac{Z_1 - Z_2}{Z_{CN}}. \tag{1}$$

Here, A_i and Z_i ($i = 1,2$) represent the mass and charge numbers of the respective fragments, and A_{CN} and Z_{CN} are the mass and charge of the compound nucleus. The temperature-dependent collective potential energy, or fragmentation potential, can be expressed using the relative spacing, R, and η-coordinates as below.

$$V(R, \eta, T) = \sum_{i=1}^{2} V_{LDM}(A_i, Z_i, T) + \sum_{i=1}^{2} \delta U_i \exp\left(-\frac{T^2}{T_0^2}\right)$$
$$+ V_C(R, Z_i, \beta_{\lambda i}, \theta_i, T) + V_N(R, Z_i, \beta_{\lambda i}, \theta_i, T)$$
$$+ V_\ell(R, Z_i, \beta_{\lambda i}, \theta_i, T). \tag{2}$$

Here ,V_{LDM} corresponds to the liquid drop part of the binding energy of Davidson *et al.* [49] and δU is the shell corrections from Myers and Swiatecki [50]; the value of T_0 =1.5 MeV is taken from classical work of Jensen and Damgaard [51], V_C, V_N, and V_ℓ are the Coulomb, nuclear interaction and angular-momentum-dependent potential for deformed and oriented nuclei.

The preformation probability of decaying fragments in η-coordinates at $R = R_a$ is determined by solving the stationary Schrodinger equation as:

$$P_0 = \sum_{\nu=0}^{\infty} |\psi^\nu(\eta(A_i))|^2 \sqrt{B_{\eta\eta}} \frac{2}{A_{CN}} \exp(-E_\eta^\nu/T), \tag{3}$$

with the ground and excited state solutions given by $\nu = 0, 1, 2, \cdots$ and the smooth hydrodynamical mass parameter represented by $B_{\eta\eta}$[52].

On the other hand, the barrier penetration probability, P, of decaying fragments is determined using the WKB integral:

$$P = \exp\left[-\frac{2}{\hbar} \int_{R_a}^{R_b} [2\mu(V(R) - Q_{eff})]^{1/2} dR\right], \tag{4}$$

with

$$V(R_a, T) = V(R_b, T) = TKE(T) = Q_{eff} \tag{5}$$

regarding the two turning points. TKE denotes the total kinetic energy, and Q_{eff} is the effective Q value.

Regarding CN decay, the following postulate is employed to describe the occurrence of the initial turning point.

$$R_a(T) = R_1(T) + R_2(T) + \Delta R(T)$$
$$= R_t(T) + \Delta R(T). \tag{6}$$

The influence of neck formation, *i.e.,* the neck length parameter, denoted $\Delta R(T)$, is described in references [53−56]. The radii are taken from references [57−61].

The temperature, T, is related to the excitation energy, E_{CN}^*, through the semi-empirical statistical relation as [62]

$$E_{CN}^* = E_{c.m.} + Q_{in} = \frac{1}{a} A_{CN} T^2 - T \text{ (MeV)}. \tag{7}$$

For this system, we have used a = 9. The entrance channel Q-value, denoted Q_{in}, is calculated using the equation $Q_{in} = B_1 + B_2 - B_{CN}$, where B_1, B_2, and B_{CN} represent the binding energies of the target, projectile, and CN, respectively [63].

For the multipole–multipole interaction between two separated nuclei, the Coulomb potential can be expressed as given in references [64−66].

The equation accounting for the influence of nuclear deformation on the radius vector ,R_i, is

$$R_i(\alpha_i, T) = R_{0i}(T) \left[1 + \sum_\lambda \beta_{\lambda i} Y_\lambda^{(0)}(\alpha_i)\right]. \qquad (8)$$

Here $i = 1,2$, $\lambda = 2,3,4$ and the variable α_i represents the angle formed between the symmetry axis and the R_i of the colliding nuclei.

In the above expression, the T-dependence nuclear radius term $R_{0i}(T)$, is given as

$$R_{0i}(T) = R_{0i}[1 + 0.007T^2]. \qquad (9)$$

Here, $R_{0i} = 1.28A_i^{1/3} - 0.76 + 0.8A_i^{-1/3}$ in femtometers.

The angular momentum effects impart additional energy to the rotational motion, and the corresponding rotational potential is computed in the references as [67, 68]. Finally, in terms of P_0 and P coordinates, the decay cross-sections are computed as follows:

$$\sigma = \frac{\pi}{k^2} \sum_{\ell=0}^{\ell_{max}} (2\ell+1)P_0 P; k = \sqrt{\frac{2\mu E_{c.m.}}{\hbar^2}}, \qquad (10)$$

where μ is the reduced mass.

The collective clusterization process within the domain of DCM is used to calculate the cross-section of CN processes, such as ER and ff (*i.e.,* σ_{ER} and σ_{ff}) as

$$\sigma_{ER} = \sum_{A_2=1}^{4} \sigma(A_1, A_2), \qquad (11)$$

$$\sigma_{ff} = 2 \sum_{A_2=A/2-20}^{A_2} \sigma(A_1, A_2), \qquad (12)$$

and for the nCN processes such as QF and FF using

$$\sigma_{QF} = \frac{\pi}{k^2} \sum_{\ell=0}^{\ell_{max}} (2\ell+1)P_{ic}, \qquad (13)$$

where P_{ic} is the penetration probability.

$$\sigma_{FF} = \frac{\pi}{k^2} \sum_{\ell_{Bf}}^{\ell_{max}} (2\ell+1)P_0. \qquad (14)$$

Here, P_0 is calculated by solving Schrodinger wave equation for fission fragments for angular momentum varying from ℓ_{Bf} to ℓ_{max}, and the barrier penetration probability is considered to be maximum (*i.e.,* $P = 1$).

Within the field, V_C and V_ℓ are widely understood, whereas V_N lacks a specific definition. Numerous theoretical frameworks exist for the computation of nuclear in-

teraction potentials. In this study, SEDF-based V_N is used to examine the stability of the heavy and superheavy mass area.

B. Skyrme Energy Density Formalism (SEDF)

The semi-classical extended Thomas–Fermi (ETF) approach [69]-based, nucleus–nucleus interaction potential in SEDF is described as

$$V_N(R) = E(R) - E(\infty), \qquad (15)$$

i.e., the potential of the interaction between two nuclei can be characterized as a function of the separation distance. $V_N(R)$ denotes the difference in the expected energy value, referred to as E, between the colliding nuclei when they are overlapping at a finite separation distance R, and when they are completely separated at $R = \infty$.

$$E = \int H(\mathbf{r})\mathrm{d}\mathbf{r}. \qquad (16)$$

The Skyrme Hamiltonian density is given as [29, 41]

$$\begin{aligned}
H(\rho, \tau, \mathbf{J}) &= \frac{\hbar^2}{2m}\tau + \frac{1}{2}t_0 \left[\left(1 + \frac{1}{2}x_0\right)\rho^2 - \left(x_0 + \frac{1}{2}\right)\left(\rho_n^2 + \rho_p^2\right)\right] \\
&+ \frac{1}{2}\sum_{i=1}^{3} t_{3i}\rho^{\alpha i} \left[\left(1 + \frac{1}{2}x_{3i}\right)\rho^2 - \left(x_{3i} + \frac{1}{2}\right)\left(\rho_n^2 + \rho_p^2\right)\right] \\
&+ \frac{1}{4}\left[t_1\left(1 + \frac{1}{2}x_1\right) + t_2\left(1 + \frac{1}{2}x_2\right)\right]\rho\tau \\
&- \frac{1}{4}\left[t_1\left(x_1 + \frac{1}{2}\right) - t_2\left(x_2 + \frac{1}{2}\right)\right](\rho_n\tau_n + \rho_p\tau_p) \\
&+ \frac{1}{16}\left[3t_1\left(1 + \frac{1}{2}x_1\right) - t_2\left(1 + \frac{1}{2}x_2\right)\right](\nabla\rho)^2 \\
&- \frac{1}{16}\left[3t_1\left(x_1 + \frac{1}{2}\right) + t_2\left(x_2 + \frac{1}{2}\right)\right] \\
&\times \left[(\nabla\rho_n)^2 + (\nabla\rho_n)^2\right] \\
&- \frac{1}{2}W_0\left[\rho\nabla.\mathbf{J} + \rho_n\nabla.\mathbf{J}_n + \rho_p\nabla.\mathbf{J}_p\right] \\
&- \left[\frac{1}{16}(t_1x_1 + t_2x_2)\mathbf{J}^2 - \frac{1}{16}(t_1 - t_2)(\mathbf{J}_p^2 + \mathbf{J}_n^2)\right].
\end{aligned} \qquad (17)$$

Here, the nuclear density, kinetic energy density, and spin–orbit density are depicted by $\rho = \rho_n + \rho_p$, $\tau = \tau_n + \tau_p$, and $\mathbf{J} = \mathbf{J}_n + \mathbf{J}_p$, and m denotes the nucleon mass. The Skyrme force parameters such as α_i, x_1, x_2, t_1, t_2, t_3, W_0, and A were fitted by Agrawal *et al.* [40, 41], referring to the modified version implemented for Skyrme interactions, including GSkI, GSkII, and SSk Skyrme interactions.

The densities in this study were determined using the

frozen density approximation [70]:

$$\rho = \rho_1 + \rho_2,$$
$$\tau(\rho) = \tau_1(\rho_1) + \tau_2(\rho_2),$$
$$\mathbf{J}(\rho) = \mathbf{J}(\rho_1) + \mathbf{J}(\rho_2), \tag{18}$$

with $\rho_i = \rho_{in} + \rho_{ip}$, $\tau(\rho_i) = \tau_1 in(\rho_{in}) + \tau_i p(\rho_{ip})$, and $\mathbf{J}(\rho_i) = \mathbf{J}(\rho_{in}) + \mathbf{J}(\rho_{ip})$.

The nuclear density, ρ_i, is calculated using the two-parameter Fermi density distribution, as reported in references [57, 58]:

$$\rho_i(r) = \rho_{0i}(T) \left[1 + \exp\left(\frac{r - R_i(T)}{a_i(T)}\right) \right]^{-1}, \tag{19}$$

with a central density of

$$\rho_{0i}(T) = \frac{3A_i}{4\pi R_i^3(T)} \left[1 + \frac{\pi^2 a_i^2(T)}{R_i^2(T)} \right]^{-1}. \tag{20}$$

Here R_i is the nuclear radius and a_i is the surface thickness parameters [57−61]. Further, the i-dependence in the nuclear radii, R_i, is shown by Eq. (9) and the T-dependence in the surface thickness parameter a_i is introduced as in references [62, 71]

$$a_i(T) = a_i(T = 0)[1 + 0.01T^2]. \tag{21}$$

In the context of V_N, we adopt the slab approximation of semi-infinite nuclear matter with parallel surfaces in the x-y plane. The slab is in motion along the z-direction and is separated by a distance, s, with a minimum separation value denoted s_0 [59, 72]. The expression for the interaction potential, $V_N(R)$, between two distant nuclei, where $R = R_1 + R_2 + s$, is given by

$$V_N(R) = 2\pi\overline{R} \int_{s_0}^{\infty} e(s)\mathrm{d}s$$
$$= 2\pi\overline{R} \int H(\rho, \tau, j) - [H(\rho_1, \tau_1, \mathbf{J}_1) + H(\rho_2, \tau_2, \mathbf{J}_2)]$$
$$= V_P(R) + V_J(R). \tag{22}$$

$\overline{R}$ is the mean curvature radius, and $e(s)$ is the interaction energy per unit area between the two slabs.

Moreover, $V_P(R)$ and $V_J(R)$ represent the components of the nuclear interaction potential that are independent and dependent on the spin density, respectively.

In this work, we have used two different approximations to calculate the reaction cross-sections. The WKB approximation and the Hill–Wheeler approximations are

two different approaches developed to calculate the barrier transmission probabilities. The Hill–Wheeler approximation is a purely parabolic barrier and is appreciated for its simplicity and numerical efficiency. However, above the barrier energies, the cross-sections merge for both approximations. Hence, we applied the Hill–Wheeler approximation to compute the capture cross-sections.

C. The ℓ-summed extended-Wong Model

The cross-section for fusion/capture between two orientated and deformed nuclei can be determined by considering the orientation angles, θ_i, and the center of mass energy, $E_{\text{c.m.}}$, of the collision in the ℓ-summed Wong model [73], which is calculated as follows in terms of angular momentum, ℓ, partial waves:

$$\sigma(E_{\text{c.m.}}, \theta) = \frac{\pi}{k^2} \sum_{\ell=0}^{\ell_{\max}} (2\ell + 1) P_\ell(E_{\text{c.m.}}, \theta), \tag{23}$$

P_ℓ is the transmission coefficient for each ℓ, which characterizes the penetration of the barrier, and $\ell_{\max}$ is the maximum angular momentum, with $k = \sqrt{\frac{2\mu E_{\text{c.m.}}}{\hbar^2}}$, and μ is the reduced mass [73].

Probability of CN formation, P_{CN}:

The probability of obtaining a completely fused compound system after the capture stage is referred to as the probability of CN formation (P_{CN}). In the superheavy mass region, the probability of formation of a CN decreases as the atomic number increases. Here, the energy dependence of fusion probability approximated by a simple relationship as [36, 43]

$$P_{\text{CN}} = \frac{P_0'}{1 + \exp\left(\frac{V_B^* - E^*}{\Delta}\right)}. \tag{24}$$

Here, V_B^* is the compound nucleus excitation energy at $E_{\text{c.m.}} \approx$ Coulomb barrier, E^* is the compound nucleus excitation energy, and $\Delta = 4$ MeV for these calculations. Moreover, the parameters used in calculating P_0' are taken from reference [43].

Fusion-fission (ff) and Quasi fission (QF) lifetimes:

Further, the lifetimes for ff and QF are examined using the theoretical approach, as given by [44, 45]

$$\tau_{\text{ff}|QF} = \frac{1}{\lambda_{\text{ff}|QF}}, \tag{25}$$

where $\lambda_{\text{ff}|QF}$ is the ff or QF decay constant and is expressed as

$$\lambda_{\text{ff}|QF} = \frac{\omega_m}{2\pi\omega_{\text{ff}|QF}} \left(\sqrt{\left(\frac{\Gamma}{2\hbar}\right)^2 + \omega_{\text{ff}|QF}^2} - \frac{\Gamma}{2\hbar} \right)$$

$$\times \exp\frac{-B_{\text{ff}|QF}}{T}. \qquad (26)$$

Here, ω_m is the frequency of the harmonic oscillator, $\omega_{\text{ff}|QF}$ refers to the frequency of the inverted harmonic oscillator, $B_{\text{ff}|QF}$ is the barrier corresponding to ff and QF, Γ denotes an average width taken as 2 MeV, and T is the temperature in megaelectronvolts.

The DCM equations were employed for the computation of cross-sections pertaining to different CN and nCN processes, as well as the determination of lifetimes associated with ff and QF, as discussed in Sec. III.

III. CALCULATIONS AND DISCUSSION

During heavy-ion processes, the nuclei contact one other as a result of Coulomb interactions. In context to the center-of-mass system, if the projectile possesses sufficient energy and the appropriate angular momentum, the nuclei can penetrate the Coulomb barrier and become confined within the potential well. This results in a compound nucleus is in a state of complete equilibrium, also known as the CN process. Alternatively, if the captured system does not undergo significant evolution within the fusion pocket, mechanisms such as QF and FF become relevant. In the present analysis, we carried out our calculations to investigate the decay mechanisms of $^{248}\text{No}^*$ and $^{250}\text{No}^*$ isotopes having $Z = 102$ nobelium nuclei over a broad range of center-of-mass energies near and above the Coulomb barrier. The DCM was used to examine the contributions of CN and nCN in fission. The interaction potential was obtained by applying the SEDF with GSkI force parameters. The included deformations extend up to the quadrupole (β_2) moment, with the optimum orientation (θ_i^{opt}). Using our detailed analysis, we aimed to study the decay mechanism (ff, QF, or FF) of the potential energy surfaces (PES); preformation factor, P_0; penetrability, P; neck length parameters; and scattering potential, V(R). Further, the capture cross-sections, were studied using the ℓ-summed Wong model for comparison with the existing experimental data. Moreover, the decay cross-sections for the above stated processes were obtained and compared with the available experimental findings [36, 37]. In addition, ff and QF lifetimes were estimated, and P_{CN} was computed.

Here, we will discuss the decay of the $^{248}\text{No}^*$ composite system formed via $^{40}\text{Ca} + ^{208}\text{Pb}$ reaction. Figure 1 shows the scattering potential at $\ell = 0\hbar$ for $^{40}\text{Ca} + ^{208}\text{Pb}$ reaction at $E_{\text{c.m.}} = 187.03$ MeV with respect to R (fm). It is crucial to note that the first turning point, R_a, (which is equal to $R_1 + R_2 + \Delta R$) represents the distance between the nuclei at which the fragments are assumed to have

already preformed and begun to penetrate the interaction barrier. Similarly, R_b, the second turning point is the point at which the process of penetrating the interaction barrier is fully completed. The QF barrier is marked and is defined as the potential difference between the barrier, V_B, and the potential at the first turning point, $V(R_a)$, which depends on the angular momentum of the incoming channel at the specified incident energy.

To evaluate the impact of different mechanisms on the synthesis of superheavy nuclei, we computed the P_{CN} for both $^{248}\text{No}^*$ and $^{250}\text{No}^*$ nuclei. If the value of $P_{\text{CN}} \sim 1$, then the reaction is classified as a CN reaction. The deviation of P_{CN} from unity indicates the potential to investigate the significance of the nCN process. The calculated P_{CN} for the two isotopes of $^{248}\text{No}^*$ and $^{250}\text{No}^*$ having $Z = 102$ nuclei with three different entrance channels, *i.e.*, $^{40}\text{Ca}+^{208}\text{Pb}$, $^{44}\text{Ca}+^{206}\text{Pb}$, and $^{64}\text{Ni}+^{186}\text{W}$ are 3.40×10^{-5}, 1.94×10^{-5}, and 1.06×10^{-5} respectively. When the value of P_{CN} is less than 1 in the calculated data, the occurrence of nCN processes is suggested. Hence, the contributions of σ_{ff}, σ_{QF}, and σ_{FF}, are obtained such that dynamics of superheavy systems can be understood.

A. Fusion–fission (ff) and nCN quasi fission (QF) and fast fission (FF) cross sections of the $^{248}\text{No}^*$ and $^{250}\text{No}^*$ nuclei.

Experimental data were employed to assess the ff, QF, and FF cross-sections for the $^{248}\text{No}^*$ and $^{250}\text{No}^*$ nuclei. These calculations were performed via the DCM framework. Additionally, the capture cross-section (σ_{capture}) was studied by utilizing the ℓ-summed Wong model. The calculations were carried out by considering the hot optimum orientations at the energies around the
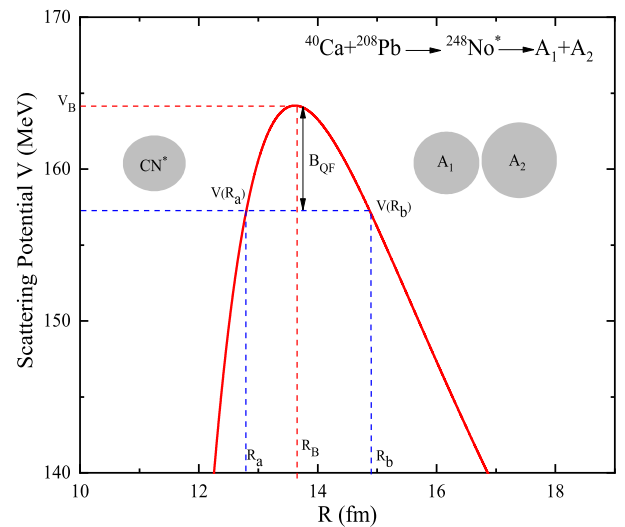

Fig. 1. (color online) Calculated scattering potential, V (MeV), as a function of range, R (fm), for the entrance channel of $^{248}\text{No}^*$ nuclei at $\ell = 0\hbar$ at $E_{\text{c.m.}} = 187.03$ MeV.

barrier of the decay fragments. Initially, we discuss the ^{248}No* nucleus. Figure 2 shows the fragmentation potential, V (MeV), for the decay of ^{248}No* nuclei at three $E_{\text{c.m.}}$ = 187.03, 209.67, and 239.03 MeV for the $\ell_{\max}$ values of angular momentum obtained from the most probable fragment for which the penetrability becomes equal to one (*i.e.*, $P = 1$). The T-dependent collective potential energy calculation provides information about the relative contributions of potential decay fragments. (i) From the figure, it is evident that with increase in temperature, the magnitude of the fragmentation potential increases, whereas the structure remains similar as we move from lower energies to the higher excitation energies. (ii) The most probable decaying fragments are clearly indicated in the figure, and it can be seen that the decay fragments remain the same independent of the expectation energy. (iii) The angular momentum for the highest $E_{\text{c.m.}}$ is greater than for the other $E_{\text{c.m.}}$ values, which could be attributed to the fact that a higher $E_{\text{c.m.}}$ requires more angular momentum to decay. (iv) The configuration of fragmentation potential for light mass fragments (LPs) and intermediate mass fragments (IMFs) and the fission region remains similar at extreme energies.

Figure 3 delves deeper into the examination of decay by plotting the preformation probability (P_0) based on the fragment mass, A_i ($i = 1,2$). The analysis illustrates that the fission contribution becomes more pronounced as the ℓ values increase. When examining the preformation profile at different $E_{\text{c.m.}}$, it is clear that the value of P_0 varies, whereas the distribution of mass for the fission fragments remains nearly equal and is asymmetric, regardless of the $E_{\text{c.m.}}$. Crucially, these secondary peaks can be linked to

the potential for the QF process. Further, the most probable fragments and their complimentary fragments observed on the asymmetric peaks remain similar as we move from the lowest to the highest $E_{\text{c.m.}}$. Furthermore, we emphasize that the fragment with maximum probability to be preformed is ^{120}Sn and its complementary fragment, ^{128}Te. Both emitted fragments are near the magic numbers $Z = 50$ and $N = 82$, and hence, the shell effects are key to the asymmetric fission distribution.

Based on our understanding of the potential for fragmentation and the preformation analysis, we aimed to analyze the conflicting CN and nCN decay processes in the ^{248}No* nucleus. A recent investigation involved examining the decay mechanism of $Z = 102$ nuclei using ^{40}Ca + ^{208}Pb reaction with DCM. σ_{capture} incorporates the contributions from CN and nCN processes, *i.e.*, $\sigma_{\text{capture}} = \sigma_{\text{CN}} + \sigma_{\text{nCN}}$. The current study focuses on the σ_{capture} for the ^{248}No* nucleus corresponding the $E_{\text{c.m.}}$ calculated using the ℓ-summed Wong Model, and the $\ell_{\max}$ values are determined via the sharp cutoff model [74]. Table 1 clearly shows that σ_{capture} increase with the increase in $E_{\text{c.m.}}$. The conclusions derived within the theoretical approach are consistent with the experimental data. Additionally, the formation of a compound system involves two components: the ER and ff cross-sections. Mathematically, this can be expressed as $\sigma_{\text{CN}} = \sigma_{\text{ER}} + \sigma_{\text{ff}}$. Alternatively, we can address the hindrance in the CN formation by considering the nCN cross-sections (σ_{nCN}), which consider the contributions of both QF and FF processes. In other words, we can express σ_{nCN} as the sum of σ_{QF} and σ_{FF}. Thus, we examined CN-fission. The fragments chosen for ^{248}No* nuclei were within the limits of
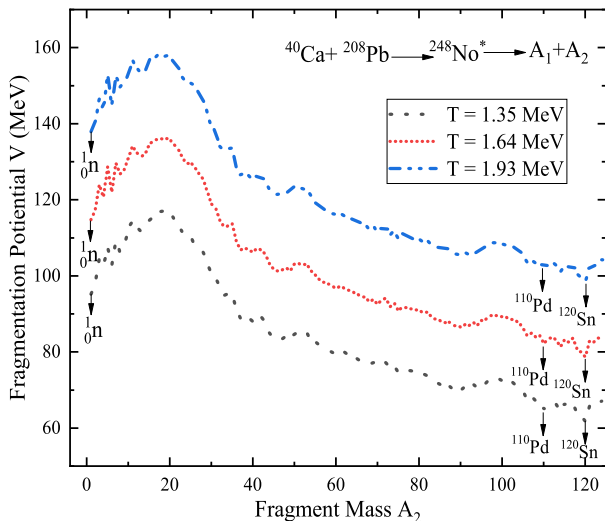

Fig. 2. (color online) Fragmentation potential, V(A_2), for the ^{248}No* nuclear system formed via the ^{40}Ca + ^{208}Pb reaction system at $E_{\text{c.m.}}$ = 187.03, 209.67, and 239.03 MeV, using the fixed value of ΔR for the maximum $\ell_{\max}$ values of the angular momentum.
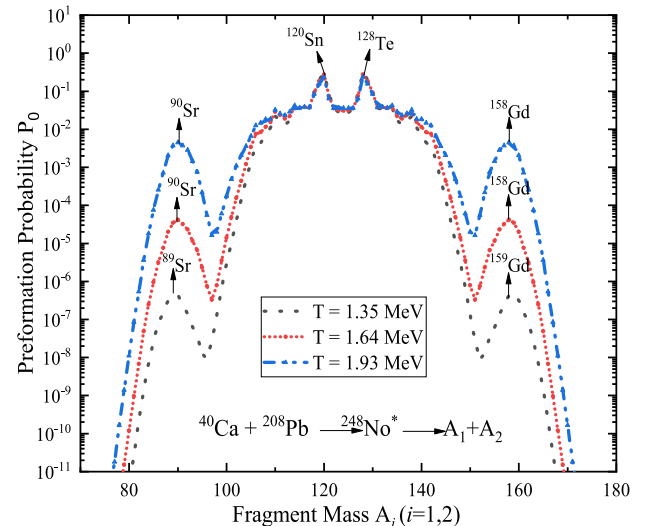

Fig. 3. (color online) Fragment preformation probability, P_0, versus the fragment mass A_i ($i = 1,2$) for the decay of ^{248}No* nuclei including the β_2-deformation effects, plotted with a fixed neck-length parameter and the highest value of the angular momentum.

$A/2 \pm 20$ for correspondence with existing data.

In the QF phenomenon, the projectile is captured by the target nucleus and a non-equilibrated compound system is formed. This system remains confined within the potential well for a brief period. The QF contributions are calculated by considering the most probable fragments that appear on the shoulders of the preformation probability, P_0, from Fig. 3, and their complementary fragments, and further considering the preformation probability of each fragment on the peak and distributing the probability among all the considered fragments. The FF process results in the formation of a mononucleus that has successfully withstood the QF process. Of note, the angular momentum of the mononucleus is significant. At high angular momentum, the rotating system's fission barrier becomes insignificant because of the enhanced rotational energy. Therefore, a highly energetic and rapidly rotating nucleus experiences rapid fission, resulting in the production of two fission fragments, which resemble those produced in the FF process. For fission fragments (A_2 = 90–124 and the complementary fragments), the Schrodinger equation must be solved to obtain the P_0 for FF. The ℓ values range from ℓ_{Bf} to ℓ_{max}, where ℓ_{Bf} denotes the angular momentum at which the fission barrier ceases to exist. In this case, the possibility of barrier penetration is deemed to be maximal, i.e., $P = 1$. Clearly, Table 1 shows that the contribution of the CN process from ff first increases and then decreases as we move from lowest to highest $E_{c.m.}$, whereas in nCN processes, i.e., QF and FF, the contribution is large at higher energies. Further, Table 1 provides the estimated cross-sections for the DCM, together with the associated values of ΔR, T, and ℓ_{max} values, E^*_{CN} and $E_{c.m.}$, and $\sigma_{capture}$ obtained by employing the ℓ-summed Wong model for the decay of the ^{248}No* nucleus. The DCM-derived cross-sections of the ff, QF, and FF processes and capture cross-sections show excellent concordance with the experimentally obtained data at all energy levels. Moreover, we obtained the $2n$ channel evaporation cross-sections for ^{248}No* nuclei. The aforementioned observed cross-sections were determined by the optimization of ΔR. Accounting for the contribution of ΔR in the decay process is crucial because it leads to shape elongation in the compound system, resulting in the development of a neck between the nascent frag-

ments. The presence of a neck region in the dinuclear system allows for the free movement of nucleons between the nuclei. This creates an opportunity for significant exit channels by altering the interaction barrier [75, 76]. The flow of mass drift and the adjustment of the barrier are governed by the neck length, ΔR. According to Fig. 4, there is a clear correlation between the increase in ΔR and an increased $E_{c.m.}$. Further, as a result of its lower-barrier characteristics, the extended GSkI force necessitates a greater ΔR value, but it remains within the maximum allowable value. The value of ΔR gives an idea about the temporal scale of the fragments' reaction time; that is, the reaction time will be faster when the value of ΔR is higher. Because the QF process takes place faster than the ff and FF, ΔR is slightly higher for QF than the ff and FF.

Further, the impact of different entrance channel mass asymmetries on the synthesis of ^{250}No* nucleus was assessed. This was achieved by considering two different incoming channels: ^{44}Ca + ^{206}Pb and ^{64}Ni + ^{186}W, at different $E_{c.m.}$ = 187.04 and 231.38 MeV. A comparison of the fragmentation potential, V (in MeV), is presented versus fragment mass in Fig. 5. The fragmentation potential shows a roughly identical variation for both entrance channels, with a slightly greater magnitude seen for the ^{44}Ca + ^{206}Pb case compared to ^{64}Ni + ^{186}W. The deformation effect shows the asymmetric nature of the fragmentation potential for both considered entrance channels in the analysis. According to the calculations based on the DCM, the fragmentation characteristics of ER, IMF, heavy HMF, and fission fragments are nearly identical. This means that the choice of entrance channel does not have any significant impact on the fragmentation behavior. Furthermore, the minima in the fragmentation potential for both entrance channels show a similar pattern. The results are elucidated in relation to the relative preformation probability, P_0. Figure 6 illustrates the computed preformation probability for the decay of ^{250}No* at different ℓ_{max} values and their corresponding $E_{c.m.}$ values. As shown, the preformation probability shows a slight variation in magnitude for the different entrance channels, whereas the structure remains almost similar and even overlaps each other in the fission region irrespective of the choice of entrance channels. Additionally, both cases have almost symmetrical fission peaks, and the con-

Table 1. DCM-measured evaporation residue, σ_{2n}, fusion-fission, σ_{ff}, quasi-fission σ_{QF}, and fast fission, σ_{FF} cross-sections; as well as capture cross-sections, $\sigma_{capt.}$; as calculated using the ℓ-summed Wong Model for ^{248}No* nucleus at different $E_{c.m.}$, along with the relevant ΔR, T, and ℓ_{max} values, compared with experimental data [36].

$E_{c.m.}$ /MeV	E^*_{CN} /MeV	T /MeV	ℓ_{max} /$\hbar$	ΔR /fm	σ^{DCM}_{2n} /nb	σ^{DCM}_{ff} /mb	$\sigma^{Expt.}_{ff}$ /mb	ΔR_{QF} /fm	σ^{DCM}_{QF} /mb	$\sigma^{Expt.}_{QF}$ /mb	ΔR_{FF} /fm	σ^{DCM}_{FF} /mb	$\sigma^{Expt.}_{FF}$ /mb	$\sigma^{DCM}_{capt.}$ /mb	$\sigma^{Expt.}_{capt.}$ /mb
187.03	49	1.35	123	2.14	0.00771	160.11	159	2.27	53.49	53	−	−	−	212.0	212
209.67	73	1.64	134	2.21	11.3	306.25	305	2.29	62.90	62	1.58	253.35	253	627.35	620
238.19	101	1.93	147	2.22	442	280.23	280	2.30	79.10	79	1.77	575.44	572	939.96	931

tributing fission fragments remain the same. Furthermore, the fragments with maximum probability to be pre-formed, *i.e.*, ^{122}Sn and its complementary fragment ^{128}Te are close to $Z = 50$ and $N = 82$ magic shell closure. Table 2 provides information related to the various decay modes and their corresponding cross-sections, ℓ_{max} values, neck length parameter for for both incoming channels obtained using the GSkI force parameters. Table 2 clearly demonstrates that the ℓ_{max} values and the ΔR are comparable for both incoming channels. This suggests that the decay of ^{250}No* is not influenced by entrance channel effects. In addition, the calculations reveal that
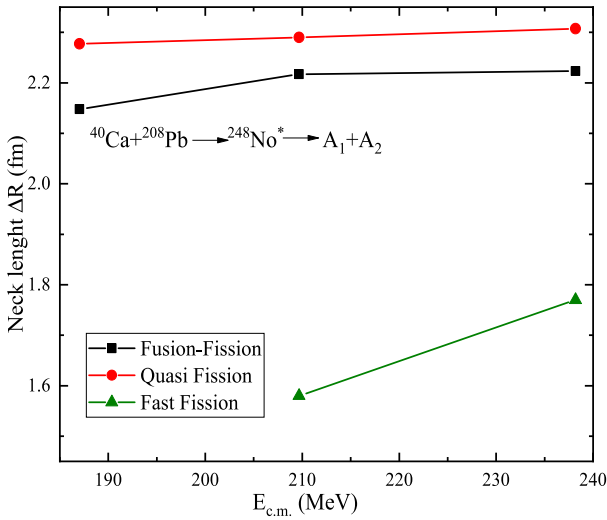
the contribution of the CN ff process is greater in the case of the ^{44}Ca + ^{206}Pb reaction, whereas the nCN QF process appears to compete with ff in the ^{64}Ni + ^{186}W reaction channel. Ultimately, the investigation of the decay of ^{250}No* resulting from the collision of ^{44}Ca and ^{64}Ni beams with ^{206}Pb and ^{186}W targets, respectively, was carried out using the DCM framework, considering the impact of deformation. From the findings, it can be concluded that the decay process is independent of formation approach or range of excitation energies.

B.   Fusion-fission (ff) and quasi-fission (QF) lifetimes:

This subsection focuses on the lifetimes of the ff and QF processes. Fission is a dynamic phenomenon where the nucleus undergoes deformation until it reaches a point of scission. Regarding significance, the timescale of the induced fission process is crucial, both theoretically and experimentally, because it is key to comprehend the nuclear reaction process. The overall duration of a fission process can be conceptually separated into two primary components: the time required for the nucleus to cross the saddle point, and the time it takes for the nucleus to deform from the saddle point to the scission point. The QF barrier depends upon the $Z_1 Z_2$ product, which in turn influences its lifetime. Hence, the available time may not be sufficient for conversion into a CN, resulting in the occurrence of the QF process. As a result, the duration of a partially equilibrated nuclear complex should be shorter than that of a fully equilibrated compound nuclear channel. Thus, the fission rate and fission lifetime for the asymmetric reaction, such as ^{40}Ca + ^{208}Pb, ^{44}Ca + ^{206}Pb and symmetric ^{64}Ni + ^{186}W reactions, which leads to the formation of ^{248}No* and ^{250}No* having $Z = 102$ nuclei, were calculated. Table 3, shows the comparison of ff and

Fig. 4.   (color online) Neck length parameter, ΔR (fm), with respect to $E_{c.m.}$ (MeV) optimized for ff, QF, and FF using the GSkI Skyrme force.

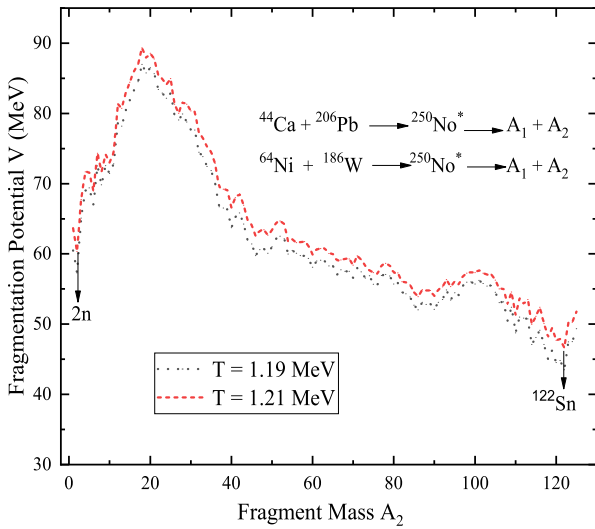**Fig. 5.**   (color online) Variation of Fragmentation potential, $V(A_2)$, for the parent nucleus ^{250}No* formed in the ^{44}Ca + ^{206}Pb and ^{64}Ni + ^{186}W reaction channels at ℓ_{max} values and best-fitted values of the neck length parameter, ΔR.
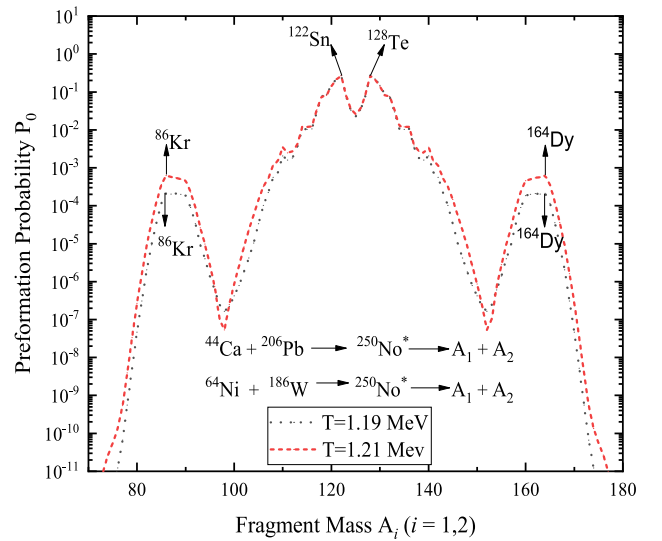

Fig. 6.   (color online) Same as Fig. 5 but the preformation probability, P_0, varies with fragment mass, A_i ($i = 1,2$).

Table 2. DCM-calculated fusion fission, σ_{ff}, quasi-fission, σ_{QF}, and fast-fission, σ_{FF}, cross-sections; as well as capture cross-sections $\sigma_{capt.}$ calculated using the ℓ-summed Wong Model in the decay of ^{250}No* nucleus formed in ^{44}Ca + ^{206}Pb and ^{64}Ni + ^{186}W reaction channels at different center-of-mass energies, $E_{c.m.}$, with the best fitted neck length ΔR, T, and ℓ_{max} values.

Reaction	$E_{c.m.}$/MeV	E_{CN}^*/MeV	T/MeV	$\ell_{max}/\hbar$	ΔR_{ff}/fm	σ_{ff}/mb	ΔR_{QF}/fm	σ_{QF}/mb	$\sigma_{capt.}$/mb
^{44}Ca + ^{206}Pb	187.04	38.69	1.19	85	2.19	109.34	2.33	27.23	140
^{64}Ni + ^{186}W	231.38	40	1.21	86	2.10	22.54	2.41	66.99	89.7

Table 3. Comparison of fusion–fission lifetime, τ_{ff}, and quasi-fission lifetime, τ_{QF}, for different formation reactions of ^{248}No* and ^{250}No* at different excitation energies using the DCM and DNS approach.

Reaction	$E_{c.m.}$/MeV	E_{CN}^*/MeV	T/MeV	τ_{ff} (DCM)/s^{-1}	τ_{ff} (DNS)/s^{-1}	τ_{QF} (DCM)/s^{-1}	τ_{QF} (DNS)/s^{-1}
^{40}Ca + ^{208}Pb	187.03	49	1.35	1.64×10^{-16}	4.98×10^{-19}	3.42×10^{-21}	5.41×10^{-21}
	209.67	73	1.64	6.91×10^{-16}	2.39×10^{-19}	3.68×10^{-21}	3.12×10^{-21}
	238.19	101	1.93	1.52×10^{-15}	1.45×10^{-19}	3.93×10^{-21}	2.14×10^{-21}
^{44}Ca + ^{206}Pb	187.04	38.69	1.19	5.49×10^{-17}	1.50×10^{-18}	3.01×10^{-21}	1.46×10^{-20}
^{64}Ni + ^{186}W	231.38	40	1.21	4.85×10^{-17}	1.18×10^{-18}	1.18×10^{-21}	1.41×10^{-21}

QF lifetime τ_{ff} / τ_{QF} using the E_{CN}^* within the DCM and DNS approaches [73, 74]. The DCM and DNS approaches use different parameters to calculate the lifetime, thus leading to the observed difference in magnitude. In the DCM, the lifetime depends on three major factors, $i.e.$, the preformation probability, P_0, penetrability, P, and barrier assault frequency, ν_0, whereas in DNS approach is greatly influenced by the charge number of the projectile and target nuclei, beam energy, etc. As shown in Table 3, the calculations carried out for the DNS cases are consistent with the trend that lifetime decreases with the increase in the excitation energy E_{CN}^*, whereas in DCM analysis, the lifetime remains almost constant. There is a noticeable trend that ff and QF lifetime τ_{ff} / τ_{QF} decreases with increase in the E_{CN}^*. Therefore, the stability of a massive CN decreases as its excitation energy increases, primarily because the fission barrier is reduced. On comparing the lifetimes obtained using the DCM and DNS approaches, there is a small magnitude difference for the ff channel, whereas the QF lifetimes are almost the same for both approaches. Thus, the chance for survival of the large CN decreases as the fission barrier falls with the increase in the E_{CN}^* of the resulting compound system.

IV. SUMMARY AND CONCLUSIONS

Using the DCM, the competing decay mechanisms (ff, QF, and FF) leading to ^{248,250}No* isotopes having $Z =$ 102 nucleus reactions were investigated using CN and nCN processes. The investigation was conducted at incident energies around the barrier, considering the quadrupole deformation using the optimum orientation approach. The calculated ff, QF, FF, and capture cross-sections showed satisfactory agreement with the experimental data. The existence of the nCN channel is regulated by the capture process. Further, the CN formation probability ($P_{CN} < 1$) clarifies that nCN processes, such as QF and FF, compete with the CN ff process. A comparative analysis was conducted to assess the fragmentation and preformation profiles of the isotopes ^{248}No* and ^{250}No*. The contribution of QF and FF start competing with the ff process at energies around the barrier because of the reduction in the fission barrier. The most probable fragments in mass distribution have been identified near the magic shell closure at $Z = 50$ and $N = 82$ leading to asymmetric fragmentation. Finally, the ff and QF lifetimes were estimated and compared with the DNS approach.

References

[1] S. Hofmann, V. Ninov, F. P. Hebberger *et al.*, Z. Phys. A **354**, 229 (1996)

[2] S. Hofmann, Rep. Prog. Phys. **61**, 636 (1998)

[3] S. Hofmann, Acta Phys. Polon. B **30**, 621 (1999)

[4] Yu. Ts. Oganessian, Nature **400**, 242 (1999)

[5] Yu. Ts. Oganessian, Rad. Phys. Chem. **61**, 259 (2001)

[6] Yu. Ts. Oganessian, Pure Appl. Chem. **78**, 889 (2006)

[7] Yu. Ts. Oganessian, J. Phys. G **34**, R165 (2007)

[8] Yu. Ts. Oganessian, Nucl. Phys. A **834**, 331c (2010)

[9] P. H. Heenen, J. Skalski, A. Staszczak *et al.*, Nucl. Phys. A **944**, 415 (2015)

[10] Yu. Ts. Oganessian, A. Sobiczewski, and G. M. TerAkopian, Phys. Scr. **92**, 023003 (2017)

[11] U. L. Businaro and S. Gallone, Nuovo Cimento **5**, 315

(1957)

[12] K. T. Davies and A. J. Sierk, Phys. Rev. C **31**, 915 (1985)
[13] D. J. Hinde, M. Dasgupta, J. R. Leigh *et al*., Phys. Rev. Lett. **74**, 1295 (1995)
[14] R. K. Gupta, M. Balasubramaniam, R. Kumar *et al*., J. Phys. G: Nucl. Part. Phys. **32**, 345 (2006)
[15] B. B. Singh, M. K. Sharma, and R. K. Gupta, Phys. Rev. C **77**, 054613 (2008)
[16] M. Bansal, S. Chopra, R. K. Gupta *et al*., Phys. Rev. C **86**, 034604 (2012)
[17] R. Kumar and R. K. Gupta, Phys. Rev. C **79**, 034602 (2009)
[18] R. Kumar and D. Jain, Nucl. Phys. A **929**, 169 (2014)
[19] S. K. Arun, R. Kumar, and R. K. Gupta, J. Phys. G: Nucl. Part. Phys. **36**, 085105 (2009)
[20] R. K. Gupta, Niyti, M. Manhas *et al*., J. Phys. G: Nucl. Part. Phys. **36**, 115105 (2009)
[21] Niyti, R. K. Gupta, and W. Greiner, J. Phys. G: Nucl. Part. Phys. **37**, 115103 (2010)
[22] M. K. Sharma, S. Kanwar, G. Sawhney *et al*., Phys. Rev. C **85**, 064602 (2011)
[23] M. K. Sharma, S. Kanwar, G. Sawhney *et al*., J. Phys. G: Nucl. Part. Phys. **38**, 055104 (2012)
[24] K. Sandhu, M. K. Sharma, and R. K. Gupta, Phys. Rev. C **85**, 024604 (2012)
[25] K. Sandhu, M. K. Sharma, and R. K. Gupta, Phys. Rev. C **86**, 064611 (2012)
[26] K. Sandhu, G. Kaur, and M. K. Sharma, Nucl. Phys. A **921**, 114 (2014)
[27] R. K. Gupta, Niyti, M. Manhas *et al*., Int. J. Mod. Phys. E **18**, 601 (2009)
[28] K. Sandhu and M. K. Sharma, Braz. J. Phys. **44**, 64 (2014)
[29] D. Jain, R. Kumar, and M. K. Sharma, Phys. Rev. C **85**, 024615 (2012)
[30] Vijay, N. Grover, K. Sharma *et al*., Phys. Rev. C **106**, 064609 (2022)
[31] Niyti, R. K. Gupta, and P. O. Hess, Nucl. Phys. A **938**, 22-44 (2015)
[32] Y.-H. Zhang, G. Zhang, J.-J. Li *et al*., Phys. Rev. C **106**, 014625 (2022)
[33] T. Bayram and A. Hayder, Phys. of Atom. Nucl. **85**(3), 275 (2022)
[34] M. S. Tezekbayeva, A. V. Yeremin, A. I. Svirikhin *et al*., Eur. Phys. J. A **58**, 52 (2022)
[35] A. V. Isaeva, A. V. Andreeva, M. L. Chelnokova *et al*., Phys. of Part. and Nucl. Lett. **18**(4), (2021)
[36] E. M. Kozulin, G. N. Knyazheva, A. A. Bogachev *et al*., Phys. Rev. C **105**, 024617 (2022)
[37] G. N. Knyazheva, M. G. Itkis, S. V. Khlebnikov *et al*., Phys. Part. Nucl. Lett. **5**(1), (2008)
[38] G. Scamps and C. Simenenel, Nature **567**, 7736 (2018)
[39] S. Jain, R. Kumar, S. K. Patra *et al*., Phys. Rev. C **105**, 034605 (2022)
[40] B. K. Agrawal, S. Shlomo, and V. Kim Au, Phys. Rev. C **72**, 014310 (2005)
[41] B. K. Agrawal, S. K. Dhiman, and R. Kumar, Phys. Rev. C **73**, 034319 (2006)
[42] R. Kumar, M. Bansal, S. K. Arun *et al*., Phys. Rev. C **80**,

[43] W. Loveland, Phys. Rev. C **76**, 014612 (2007)
[44] S. Soheyli and M. V. Khanlari, Phys. Rev. C **94**, 034615 (2016)
[45] M. V. Khanlari and S. Soheyli, Phys. Rev. C **95**, 024617 (2017)
[46] H. J. Fink, J. Maruhn, W. Scheid *et al*., Z. Phys. **268**, 321 (1974)
[47] J. Maruhn and W. Greiner, Phys. Rev. Lett. **32**, 548 (1974)
[48] R. K. Gupta, W. Scheid, and W. Greiner, Phys. Rev. Lett. **35**, 353 (1975)
[49] N. J. Davidson, S. S. Hsiao, J. Markram *et al*., Nucl. Phys. A **570**, 61c (1994)
[50] W. Myers and W. J. Swiatecki, Nucl. Phys. A **81**, 1 (1966)
[51] A. S. Jensen and J. Damgaard, Nucl. Phys. A **203**, 578 (1973)
[52] H. Kroger and W. Scheid, J. Phys. G **6**, L85 (1980)
[53] S. Kumar and R. K. Gupta, Phys. Rev. C **55**, 218 (1997)
[54] T. Matsuse, C. Beck, R. Nouicer *et al*., Phys. Rev. C **55**, 1380 (1997)
[55] S. J. Sanders, D. G. Kovar, B. B. Back *et al*., Phys. Rev. C **40**, 2091 (1989)
[56] S. J. Sanders, Phys. Rev. C **44**, 2676 (1991)
[57] L. R. B. Elton, *Nuclear Sizes* (Oxford University Press, London, 1961)
[58] L. R. B. Elton, Proc. Phys. Soc. Lond. A **63**, 1115 (1950)
[59] R. K. Gupta, D. Singh, and W. Greiner, Phys. Rev. C **75**, 024603 (2007)
[60] J. Blsocki, J. Randrup, W. J. Swiatecki *et al*., Ann. Phys. (NY) **105**, 427 (1977)
[61] O. N. Ghodsi and M. Hassanzad, Nucl. Phys. A **987**, 369 (2019)
[62] G. Royer and J. Mignen, J. Phys. G **18**, 1781 (1992)
[63] P. Möller, A. J. Sierk, T. Ichikawa *et al*., At. Data Nucl. Data Tables **109**, 1 (2016)
[64] M. Munchow, D. Hahn, and W. Scheid, Nucl. Phys. A **388**, 381 (1982)
[65] M. J. Rhoades-Brown, V. E. Oberacker, M. Seiwert *et al*., Z. Phys. A **310**, 287 (1983)
[66] R. Aroumougame and R. K. Gupta, J. Phys. G **6**, L155 (1980)
[67] N. Cindro and D. Pocanic, J. Phys. G Nucl. part. Phys. **6**, 855 (1980)
[68] R. Aroumougame, N. Malhotra, S. S. Malik *et al*., Phys. Rev. C **35**, 994 (1987)
[69] D. Vautherin and D. M. Brink, Phys. Rev. C **5**, 626 (1972)
[70] G.-Q. Li, J. Phys. G: Nucl. Part. Phys. **17**, 1 (1991)
[71] S. Shlomo and J. B. Natowitz, Phys. Rev. C **44**, 2878 (1991)
[72] P. Chattopadhyay and R. K. Gupta, Phys. Rev. C **30**, 1191 (1984)
[73] D. L. Hill and J. A. Wheeler, Phys. Rev. **89**, 1102 (1953)
[74] M. Beckerman, J. Ball, H. Enge *et al*., Phys. Rev. C **23**, 1581 (1981)
[75] A. Szanto de Toledo, B. V. Carlson, C. Beck *et al*., Phys. Rev. C **54**, 3290 (1996)
[76] B. D. Wikins, E. P. Steinberg, and R. R. Chasman, Phys. C **14**, 1832 (1976)